Oceanologia (2017) 59, 473—495

Available online at www.sciencedirect.com

ScienceDirect

journal homepage: www.journals.elsevier.com/oceanologia/

ORIGINAL RESEARCH ARTICLE

Modelling of the Svalbard fjord Hornsund

Jaromir Jakacki [a,*], **Anna Przyborska** [a], **Szymon Kosecki** [a], **Arild Sundfjord** [b], **Jon Albretsen** [c]

[a] *Institute of Oceanology, Polish Academy of Sciences, Sopot, Poland*
[b] *Norwegian Polar Institute, Tromsø, Norway*
[c] *Institute of Marine Research, Bergen, Norway*

Received 14 July 2016; accepted 5 April 2017
Available online 20 May 2017

KEYWORDS
Hydrodynamic model;
Fjord circulation;
Heat and salt content and anomalies;
Hornsund model

Summary The Arctic Ocean is currently in transition towards a new, warmer state. Understanding the regional variability of oceanographic conditions is important, since they have a direct impact on local ecosystems. This work discusses the implementation of a hydrodynamic model for Hornsund, the southernmost fjord of western Svalbard. Despite its location, Hornsund has a stronger Arctic signature than other Svalbard fjords. The model was validated against available data, and the seasonal mean circulation was obtained from numerical simulations. Two main general circulation regimes have been detected in the fjord. The winter circulation represents a typical closed fjord system, while in summer the fresh water discharge from the catchment area generates a surface layer with a net flow out of Hornsund. Also described are the local hydrographic front and its seasonal variability, as well as the heat and salt content in Hornsund. The integration of salt and heat anomalies provides additional information about the

Abbreviations: A4, 4-km resolution Pan-Arctic model (based on ROMS); ADCP, Acoustic Doppler current profiler; AO, Arctic Ocean; AW, Atlantic Water; AWAKE, Projects (including the AWAKE-2 — Arctic Climate System Study of Ocean, Sea Ice and Glaciers Interactions in Svalbard Area); GAME, Growing of the Arctic Marine Ecosystem project; GLAERE, Glaciers as Arctic Ecosystem Refugia project; ERAi, ERA-Interim — a global atmospheric reanalysis; HOBO, temperature and pressure sensor; HRM, high resolution numerical model of the Hornsund; HYCOM, Hybrid Coordinate Ocean Model; SCA, Salt Content Anomaly; KNOW, The Leading National Research Centre; MIKE, MIKE by DHI — software from the Danish Hydrological Institute; MIKE HD, Mike Flow Model, Hydrodynamic module; NavSim, NavSim Polska sp. z o.o. — Polish Dealer of the Canadian branch of this marine software company; ModOIE, Mesoscale modelling of Ice, Ocean and Ecology of the Arctic Ocean; NPI, Norway Polar Institute; ROMS, Regional Ocean Modelling System; S800, 800 m Svalbard area model (based on ROMS); SC, Sorkapp Current; TOPEX/POSEIDON, Ocean Surface Topography from Space — NASA; TOPAZ4, an ocean-sea ice data assimilation system for the North Atlantic and Arctic global TPXO model of ocean tides; WSC, West Spitsbergen Current.

* Corresponding author at: Institute of Oceanology, Polish Academy of Sciences, Powstańców Warszawy 55, Sopot, Poland. Tel.: +48 587311903.
E-mail address: jjakacki@iopan.gda.pl (J. Jakacki).

Peer review under the responsibility of Institute of Oceanology of the Polish Academy of Sciences.

Production and hosting by Elsevier

http://dx.doi.org/10.1016/j.oceano.2017.04.004

salt flux into the innermost basin of the fjord - Brepollen during the summer. Extensive *in situ* observations have been collected in Hornsund for the last two decades but our hydrodynamic model is the first ever implemented for this area. While at the moment *in situ* observations better represent the state of this fjord's environment and the location of measurements, a numerical model, despite its flaws, can provide a more comprehensive image of the entire fjord's physical state. *In situ* observations and numerical simulations should therefore be regarded as complementary tools, with models enabling a better interpretation and understanding of experimental data.

1. Introduction

Hornsund is a fjord in the south-west of the Svalbard archipelago. Its position and wide opening to Greenland Sea shelf waters (Fig. 1), as well as the large area of contact between the coastal waters and tidewater glacier fronts, expose it to the strong influence of the shelf waters. The fjord's 12 km wide mouth faces west towards the Greenland Sea. Hornsund is 30 km long with a maximum depth of about 260 m (average *ca* 90 m) (Frankowski and Zioła-Frankowska, 2014), an estimated surface area of 275 km^2 and a volume of 23 km^3. The fjord's coastline is very diverse, with a number of small bays, which are the mouths of valleys with glaciers flowing into the sea. Some of these small bays appeared as late as the beginning of the 20th century as a result of glacier recession. The area and coastline of Hornsund have been expanding gradually since the retreat of glaciers. The total area of glacier cover in Hornsund diminished from 1899 to 2010 by

Figure 1 Location of the study area — the Hornsund fjord.
Source: https://en.wikipedia.org/wiki/Svalbard (Oona Räisänen).

approximately 172 km^2, the average loss of area being 1.6 km^2 $year^{-1}$. The recession rate increased from ~1 km^2 $year^{-1}$ in the first decades of the 20th century up to ~3 km^2 $year^{-1}$ in 2001—2010 (Błaszczyk et al., 2013).

Atlantic Water (AW) supplies the biggest volume flux to the Arctic Ocean (AO) and is one of the most important factors shaping the region's climate (Walczowski, 2007, 2013). The West Spitsbergen Current (WSC) is the AW branch that has the greatest influence on conditions in Hornsund. The AW carried by this current is characterized as warm and saline (temperature *ca* 3.5—6.0°C and salinity > 35 in the surface layer off the entrance to Hornsund). But there is another current in the Hornsund area that also has a strong influence on the fjord's state. This is the Sorkapp Current (SC), which carries cold, and fresher water from the western part of the Svalbard Archipelago and the Barents Sea (temperature −1.5 to +1.5°C, salinity 34.3—34.8) (Cottier et al., 2005; Gluchowska et al., 2016). It is a typical fjord with an internal Rossby deformation radius representing the ratio of the internal wave speed to the Coriolis parameter. In the case of Hornsund we can assume that the maximum water depth is 200 m, with a surface layer (T = 4—7°C and S = 30—32) that is *ca* 20 m thick and lower layers (T = 0—4°C and S = 34—35) having an internal Rossby deformation radius between 3.5 and 6 km (Cottier et al., 2005; Nilsen et al., 2008). When the internal Rossby radius is smaller than the width of the fjord, the influence of the Earth's rotation is not insignificant. This means that variations in the flow are driven by rotational dynamics; such fjords are often called “broad”.

Tides are another process that have a strong influence on the fjord. Generally, tides are the main hydrodynamic driver in the fjord: water circulation in the fjord is governed mainly by tides and shelf currents. Tides and currents have a strong influence on the heat, salt and fresh water budgets in the fjord. The amplitude of the tidal components varies between ±0.75 m and the main component of tidal forcing in this area is the semi-diurnal (M2) constituent (Kowalik et al., 2015). Other tidal components are considered in the section on validation.

The study area has been examined previously and many experiments have been done there; indeed, much *in situ* research is still in progress (mostly Polish-Norwegian cooperative ventures), for example, AWAKE-2 (*Arctic Climate System Study of Ocean, Sea Ice and Glacier Interactions in Svalbard Area*) project, GAME (*Growing of the Arctic Marine Ecosystem*) and GLAERE (*Glaciers as Arctic Ecosystem Refugia*). Although these projects usually focus on interdisciplinary studies, *in situ* measurements do not provide a complete picture of the fjord's physical state. Typically, the observations are carried out over short timescales (for example, observations performed from a research vessel) or as long-term *in situ* measurements based on moorings. Direct measurements provide the most accurate results, but making measurements that would be representative of the whole fjord area would be very expensive and logistically difficult (apart from satellite measurements, but these cover only the surface). Another approach that could provide a complete image of the fjord's physical state is modelling. There are already many models embracing Hornsund: the Hybrid Coordinate Ocean Model (HYCOM) (Chassignet et al., 2006), which has a spatial resolution of 1/12deg; TOPAZ4 (Counillon et al., 2010; Sakov et al., 2012), which has a horizontal resolution of 10—16 km and does not take into consideration all the most important factors for studies of water circulation inside fjords (like tides); the Nordic Seas HYCOM model, which has a horizontal resolution of about 4 km, to name but three. Their domains cover much larger areas and their horizontal resolutions are insufficient for studying hydrodynamic processes in Hornsund. To conclude, we could say that although modelling tools are developing rapidly, no high-resolution hydrodynamic model focused on Hornsund has yet been developed. Both the models supplying lateral boundary data cover the Hornsund area (Hattermann et al., 2016), but the fjord is covered by only a few cells, which are insufficient for providing appropriate results.

The model that we implemented for the fjord is of high resolution, but as boundary condition we used data from another (covering a larger geographical area), lower resolution model. Our high-resolution model thus extends the existing model of the Arctic by a fjord, which in the larger model is not correctly represented. In our study, we decided to use software from the Danish Hydrological Institute (MIKE by DHI, MD) as an additional tool in order to acquire a better understanding of the processes that govern the behaviour of the fjord's physical state. With the MD software one can use an unstructured grid (also known as a mesh grid) that allows a model domain of variable spatial resolution to be created, which has advantages in areas with a wide range of depths.

This paper focuses on the implementation of MD for Hornsund and is divided into five main sections. The *Introduction* is followed by the *Model description* and *Implementation*. General information, such as the horizontal and vertical grids, the model domain and bathymetry, are presented here, and all the parameters used (including parameterizations) are listed in the table. The *Boundaries* section describes the implementation of lateral boundary conditions and applied atmospheric forcing. A separate subsection addresses the inclusion of fresh water sources from glaciers and the catchment area. The validation procedures are then described in the next three subsections. Each compares model results with available data for different areas. Because of the extensive lateral boundaries, the shelf area and fjord interior are taken into account separately. Also, because of the different nature of the driving mechanism, tidal flow is dealt with in a separate validation subsection. The main findings, including a description of typical summer and winter circulation patterns, and the hydrographic front, are presented in *Results and discussion*. This section concludes with an analysis of the heat and salt anomalies. Integrated over time, these anomalies reveal that circulation in Brepollen is relatively stable and can only be disturbed by the fresh water discharged from its catchment area.

2. Model description and implementation

2.1. General information

The numerical model of Hornsund (HRM) was set up based on MIKE HD 3D software (Mike Flow Model, Hydrodynamic module, MH). This model solves Reynolds-averaged Navier—Stokes (MIKE and Doc, 2010—2014) equations (RANS) for an incompressible medium with the Boussinesq assumption and

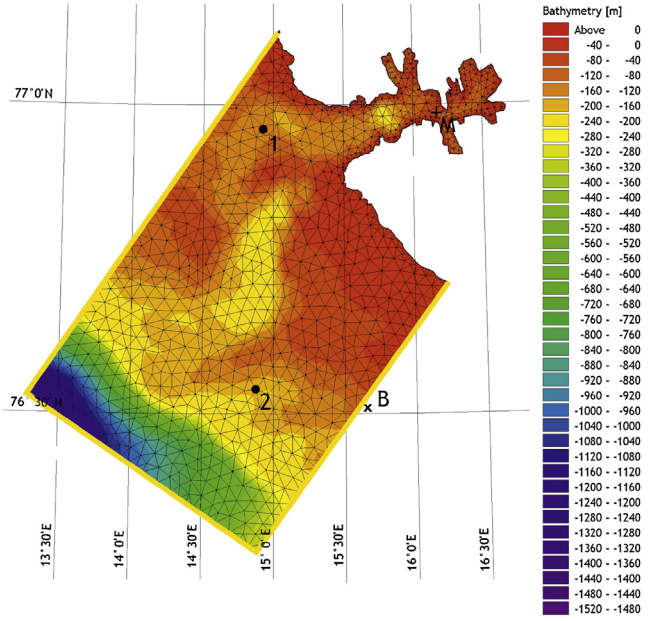

Figure 2 Model domain and bathymetry. The mesh grid, two validation points (1 and 2), the location of the thermistor string and upward looking Acoustic Doppler Current Profiler (ADCP, marked as 'M') have been marked. The solid yellow line delineates the lateral boundary and point 'B' has been inserted as a validation boundary point. (For interpretation of the references to color in this figure legend, the reader is referred to the web version of this article.)

shallow water approximation. The main parts of the model are the domain, grid and bathymetry (Fig. 2). The model's bathymetry was derived on the basis of electronic charts developed by Primar (international collaboration) and distributed by NavSim Polska sp. z o.o. (the Polish dealer of the Canadian branch of this marine software company). The above-mentioned unstructured grid enables a variable horizontal resolution to be used. The model grid consists of 2087 elements and 1293 nodes (an element is defined as a rectangle corner, and a node is the centre of the rectangle, equivalent to the grid centre in a structured grid). The smallest cell in our domain has a horizontal resolution of *ca* 300 m and the largest cell has a dimension of *ca* 3000 m. The vertical dimension of an average cell in the Hornsund area is *ca* 2.6 m (the average depth of Hornsund is about 90 m). Smaller nodes cover parts of the domain that consist of shallower water areas. The mesh grid is also shown in Fig. 2. This figure shows two validation points (points 1 and 2), and the location of the thermistor string and upward looking Acoustic Doppler Current Profiler (ADCP, the point marked 'M'). The model time step is set to 30 s (the solution technique was selected as a low-order fast algorithm). The model is based on the sigma coordinates system with 35 vertical levels. The initial temperature and salinity conditions were constant, and velocity and sea level were set to zero.

2.2. Model setup and numerical parameters

As mentioned earlier, the model solves the well-known RANS equations. However, although these equations are well known, some of the numerical features can vary and are therefore presented here. Mike by DHI is very well documented (MIKE and Doc, 2010—2014), so we provide only a table (Table 1) with the parameters used in the model.

2.3. Boundaries

The lateral boundary condition is one of the most important components of the model. It has to combine tidal forces (the internal representation does not provide the correct amplitude of sea level variation, so it has to be applied as the external sea level variation), velocity, salinity and temperature. The line of the lateral boundary is shown by the thick yellow lines in Fig. 2.

In our case three sources of data were used. Tidal forces in the Hornsund model were applied as sea level from the global tidal model (data represent the major diurnal (K1, O1, P1 and Q1) and semidiurnal tidal constituents (M2, S2, N2 and K2)) with a spatial resolution of $0.25^\circ \times 0.25^\circ$ based on TOPEX/POSEIDON altimeter data (MIKE_DHI, 2014). Barotropic velocities together with respective sea level and active tracers (temperature and salinity) were taken from two Norwegian model simulations (Hattermann et al., 2016). The coupled ocean and sea ice model is a version of the Regional Ocean Modelling System (ROMS) (www.myroms.org; Budgell, 2005; Haidvogel et al., 2008; Shchepetkin and McWilliams, 2009) with two different horizontal resolutions. The first one, the A4 model, covers a pan-Arctic domain with a 4 km resolution, while the second one (high-resolution model (S800, Albretsen et al., 2017)) is a one-way nested simulation with an 800 m resolution of the domain covering Svalbard and a large part of the Fram Strait. Both models (A4 and S800) were forced by atmospheric fields derived from ERA interim reanalysis (ERAi, Dee et al., 2011). In addition, A4 and S800 (Hattermann et al., 2016) used tidal forces retrieved from the global TPXO model of ocean tides (Egbert and Erofeeva, 2002).

The barotropic part of the boundary was specified using Flather's boundary condition (Flather, 1976):

Table 1 Parameters used in the model.

Parameter	Value	Model option or comments (if needed)
General information		
Horizontal resolution	Size of cell (max, min) = (300, 3000)	Mesh grid presented in Fig. 2
Vertical coordinates	35 vertical levels, min = ~0.2 m, max = ~40 m	Sigma coordinates
Simulation periods	01.2005–06.2010	
Maximum time step	30 s	
Bathymetry source	NavSim (based on **E**lectronic Navigational Charts – ENC)	
Flood and dry	Included	
Horizontal turbulence model	Smagorinsky	
Vertical turbulence model	$k-\varepsilon$	
Bed friction	Constant in domain, but depends on cell thickness	
Flood and dry	Included	
Density	Salinity and temperature dependent	
Coriolis forcing	Included	
Atmospheric forcing	Included	Based on ERAi: – Mean sea level pressure – Wind speed and direction – 2 m potential temperature – Cloudiness – Precipitation – Wind speed
Ice thickness and concentration	Included	Based on S800 model
Critical CFL value	0.8	Courant–Friedrichs–Lewy number
Initial conditions		Initialization from cold start
Surface level	0 m	
Velocities	0 m s^{-1}	

$$\overline{u} = \overline{u}^{ext} - \sqrt{\frac{g}{D}}(\xi - \xi^{ext}). \quad (1)$$

Computed from the Sommerfeld wave equation and the continuity equation, this condition is one of the most efficient open boundary conditions (Jeżowiecka-Kabsch and Szewczyk, 2001; Kantha and Clayson, 2000). In Eq. (1) $\overline{u}$ denotes depth-averaged velocity, D is the local depth and ξ represents sea level. The superscript *ext* links external data. The barotropic velocities in Eq. (1) were extracted and interpolated based on an 800 m ROMS setup that covers the Nordic Seas (Hattermann et al., 2016). In addition, the Dirichlet boundary was applied to temperature and salinity. The data for those variables were taken from the Nordic Seas ROMS model (4 km horizontal resolution; Lien et al., 2013).

The 2D field was interpolated for the top boundary layer. The model does not require any atmospheric data, but in order to replicate realistic conditions, we applied the following atmospheric data:

- Mean sea level pressure,
- Wind speed and direction,
- 2 m potential temperature,
- Cloudiness,
- Precipitation,
- Sea ice concentration,
- Sea ice thickness.

Atmospheric fields were prepared on the basis of the ERA Interim reanalysis data set (from the European Centre for Medium-Range Weather Forecasts) and ice coverage was taken from the S800 model.

2.4. Fresh water sources

Fresh water sources are an important part of the fjord ecosystem. The main ones include direct precipitation on to the fjord surface (taken into account as atmospheric forcing), tidewater glacier ablation and calving, melting of fast ice and sea ice, and land/riverine outflow. The fresh water sources for the Hornsund area and a compilation of the available data were presented at the Mare Nor Symposium on the Ecology of Fjords and Coastal waters (Węsławski et al., 1995). This is summarized in Fig. 3. The percentages and quantitative contributions of all fresh water components (ablation, precipitation, snow and rivers) were estimated on the basis of Fig. 3a and b. Next, the percentage contribution of each source was estimated on the basis of that report and Fig. 3b. Then, the quantitative contribution of the fresh water component for each location shown in Fig. 3b was adopted from Węsławski's results (Węsławski et al., 1995; Fig. 3a). We also introduced a time shift between the western and eastern parts of the fjord, because of the melting processes that occur in the catchment area. Moving the time period of ice melt is based on an observation provided by the Polish Polar Station in Hornsund. Melting always begins in the shelf area and then moves eastwards. The time shift between the eastern and western parts is about one month and it is not visible in the figure (Fig. 3c). Although the AWAKE2 project run by the Institute of Oceanology, Sopot, had one work

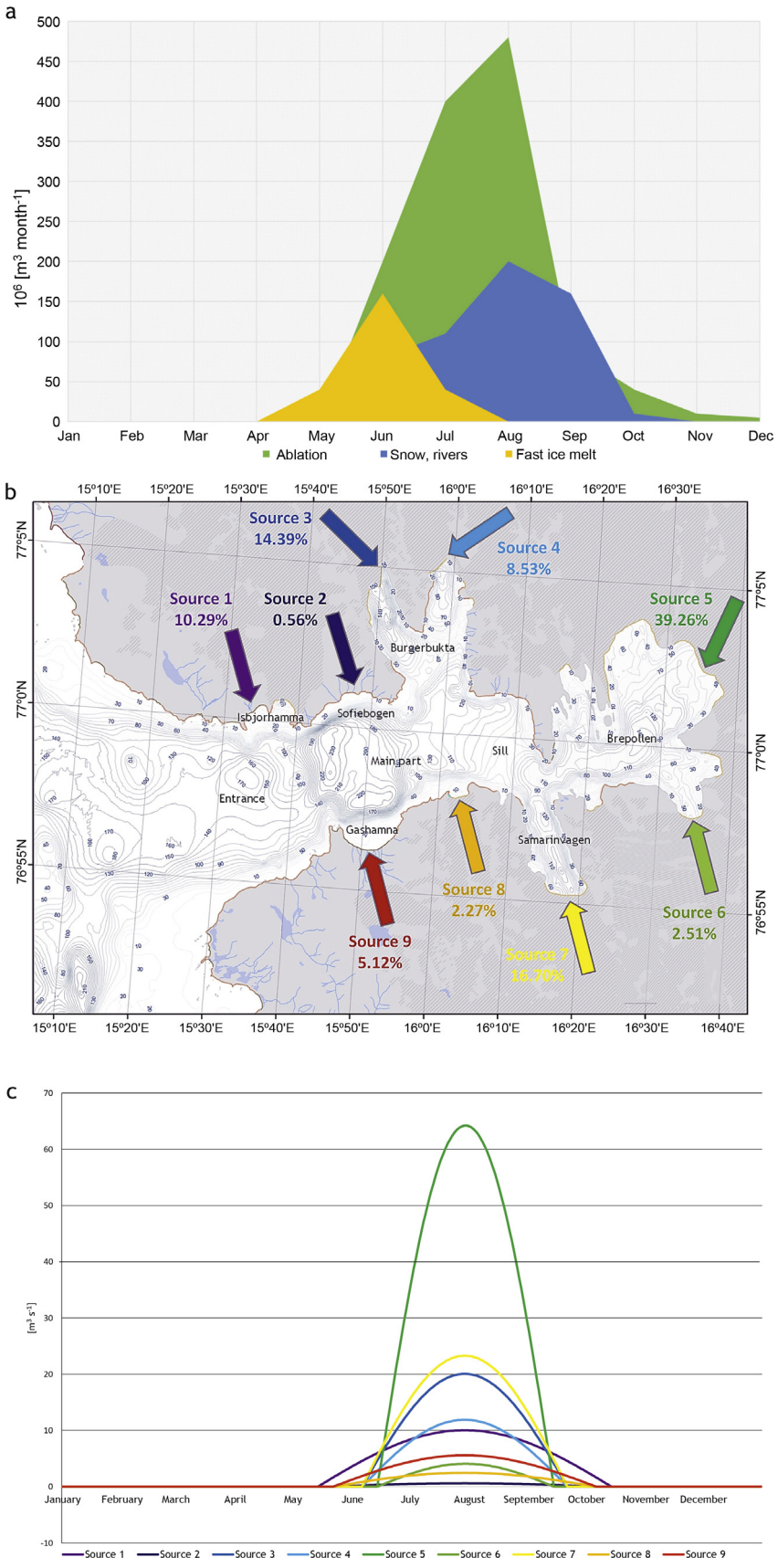

Figure 3 Sources of fresh water and their time dependence in Hornsund based on Węsławski, 1995 (a); the version implemented for the model (b) represents the estimated percentage contribution of each source; the time variability of each source (c).

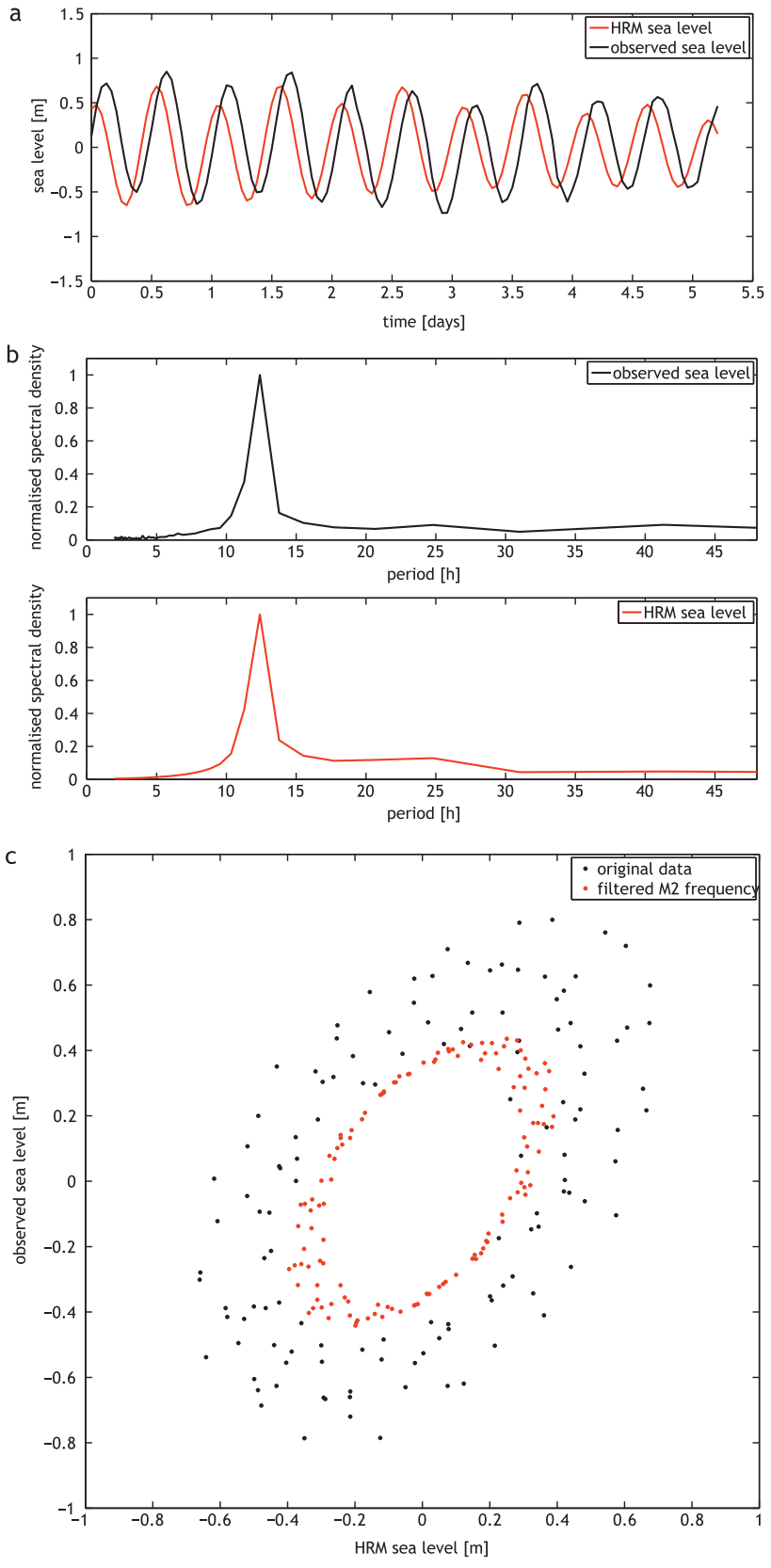

Figure 4 (a) Time series of the modelled (HRM, red line) and measured (black line) sea surface level, (b) power spectrum density derived from the time series shown in (a). The upper, black line image stands for the experimental results and the lower, red line represents the spectrum of HRM sea level; (c) comparison between measured (vertical axis) and HRM (horizontal axis) sea levels with a filtered M2 (semi-diurnal, red points) component. (For interpretation of the references to color in this figure legend, the reader is referred to the web version of this article.)

package focused on estimating fresh water sources in that area, the results are still not available. Because there are no other data that could represent fresh water from the Hornsund drainage basin, we decided to utilize the sources from Fig. 3 (Węsławski et al., 1995) in the model for the whole simulation.

3. Model validation

The validation procedure depends on the area and local forces. As validation of tidal forces requires different methods from temperature or salinity variation, it was divided into three parts:

- Tides;
- The shelf area;
- The fjord's interior.

3.1. Tide validation

The lack of experimental data does not permit long-term validation, so we used short-term measurements from the

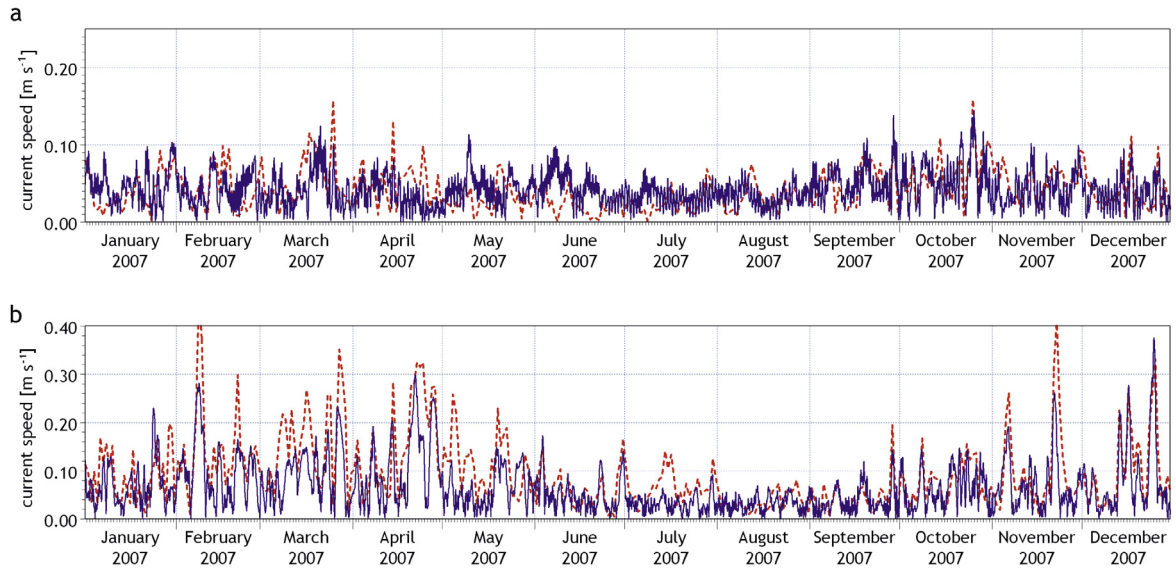

Figure 5 Comparison of barotropic current velocity at the two locations in the shelf area shown in Fig. 2 (the upper image represents point 1 (a) and the lower one point 2 (b); the blue and red lines represent the HRM and S800 models respectively). (For interpretation of the references to color in this figure legend, the reader is referred to the web version of this article.)

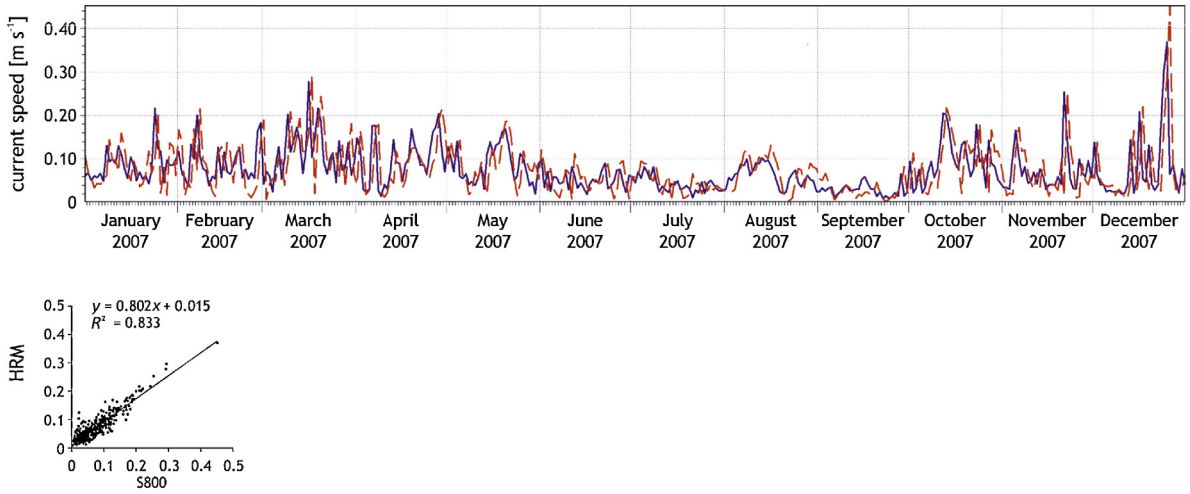

Figure 6 Comparison of the current velocity for one point located on the boundary (south-east, yellow boundary line — point 'B' in Fig. 2). The blue and red lines represent the HRM and S800 models respectively. The linear regression for this series is shown on the lower panel. Correlation coefficient $R \approx 0.91$. (For interpretation of the references to color in this figure legend, the reader is referred to the web version of this article.)

area in front of the Hansbreen Glacier measured by the Institute of Geophysics of the Polish Academy of Sciences (IGF). The *in situ* measurements were made between 9 and 15 August 2011 using a Schlumberger Mini-Diver. This instrument was equipped with a pressure sensor, and the duration of measurements was limited by its memory capacity. Our model does not provide results for those dates, but in the case of tides there will only be a phase shift between the data. Fig. 4a shows a sea level time series as measured by the Mini-Diver and the modelled one. The spectral analysis of these signals is shown in Fig. 4b. The power spectral density was normalized to the maximum of both signals (in this case to the measured maximum sea level) for better clarity. Sea levels with a filtered M2 component are compared in Fig. 4c.

Because of the different time series, the phase shift is visible in Fig. 4c as a circle (or ellipse) formed by the red points. Despite the short period covered by the *in situ* data, the results provide quite a good comparison between the measured and modelled amplitudes and frequencies. One maximum shown in Fig. 4b (period close to 12 h) represents the semidiurnal tidal constituent (M2, although there are also other semidiurnal constituents in this area), the other (close to 24 h) relates to diurnal components. However, for a short time series it is impossible to separate all the semidiurnal and diurnal constituents.

3.2. The shelf area

In the second step of the validation we compared our model data with the data provided by the S800 and A4 models. For this purpose we compared the barotropic current velocity, salinity and temperature derived from our Hornsund model with the results of models implemented as lateral boundary conditions (the comparison was performed for the two points shown in Fig. 2). Fig. 5 compares the temporal variability of the current speed derived from S800 model with that from the HRM model. The main differences can be explained by the bathymetry. All the models use different sources of bottom topography; in the case of the barotropic velocity it is the main reason for these differences. Linear correlation between these series yields low values of the coefficient that are close to 0.3. This might suggest that the lateral boundary condition has been implemented incorrectly. Except for the point located on the south-east boundary line (point 'B') on the yellow line in Fig. 2, the correlation is much better. The value of the coefficient is about 0.91 and is shown in Fig. 6. This confirms the earlier suggestion that the differences between S800 and HRM in the shelf area mostly result from differences in bathymetries.

Fig. 7 shows a time series of surface salinity and temperature derived from the HRM and A4 models. The solid lines

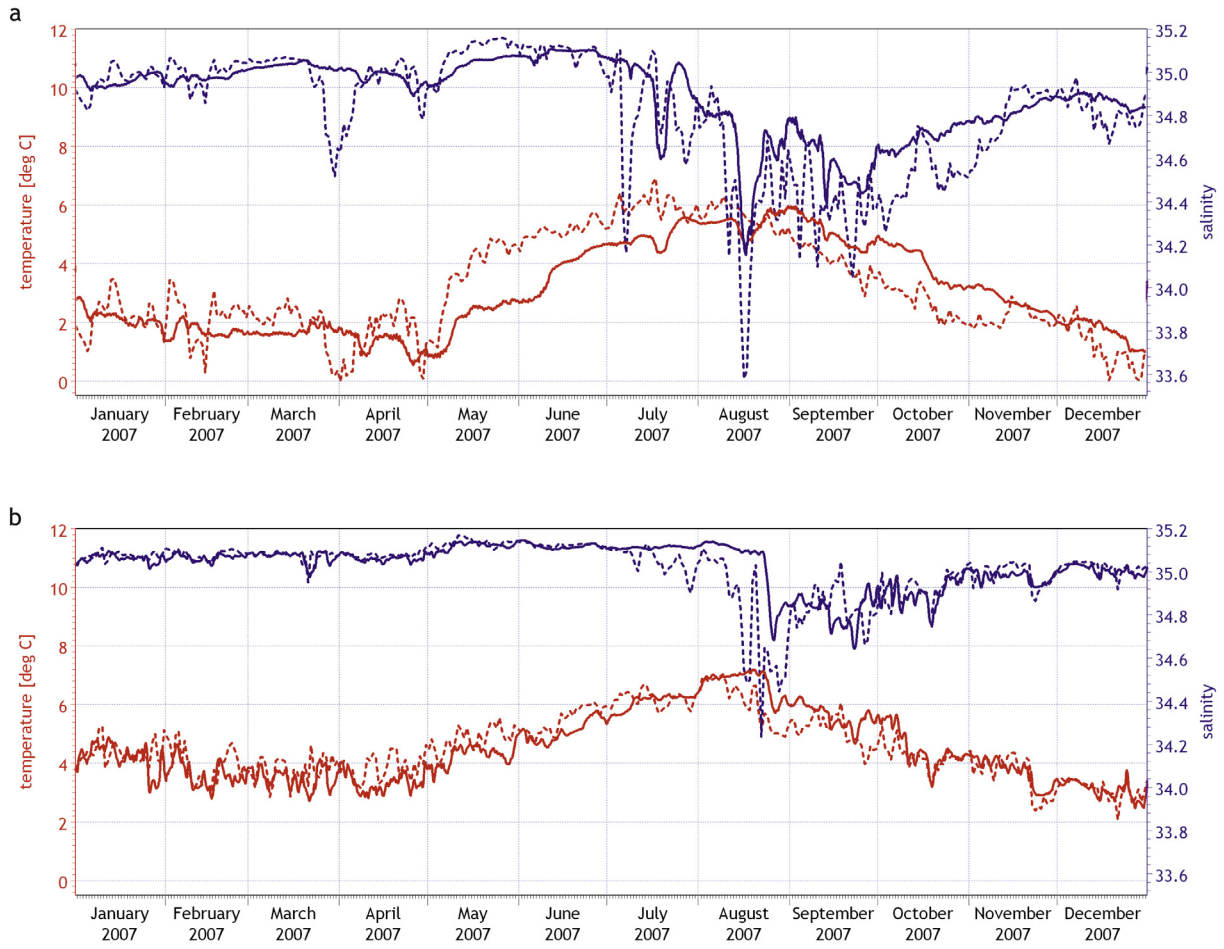

Figure 7 Comparison of temperature and salinity in the surface layer (the upper graph represents point 1 (a), the lower graph point 2 (b); the red and blue lines represent temperature and salinity respectively; the dashed lines represent model A4, the solid lines HRM). (For interpretation of the references to color in this figure legend, the reader is referred to the web version of this article.)

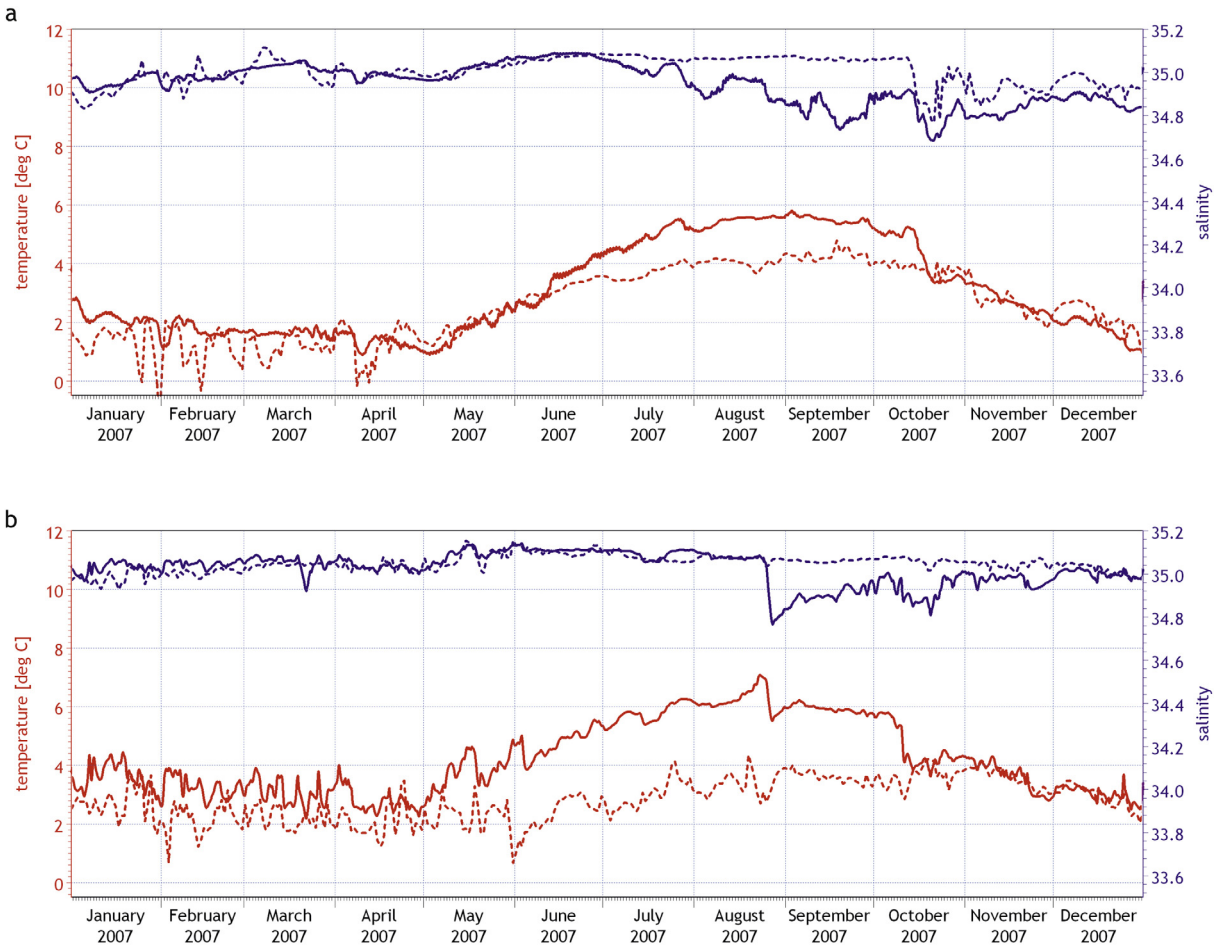

Figure 8 Comparison of temperature and salinity in the bottom layer (the upper graph represents point 1 (a), the lower graph point 2 (b); the red and blue lines represent temperature and salinity respectively; the dashed lines represent model A4, the solid lines HRM). (For interpretation of the references to color in this figure legend, the reader is referred to the web version of this article.)

refer to our HRM model. The comparison for the surface layer looks quite good. Model A4 has a 4 km resolution, so the fjord has only several points in it. In our case the main differences are between May and October, when fresh water sources were active throughout the fjord. Moreover, it is plainly evident that the model reproduces the seasonal variability of the shelf area. Fig. 8 shows a similar graph, but for the bottommost layer. Here, there is also good agreement between the results of the two models, although the temperature is a little higher for the second point in summer.

Table 2 Correlation coefficient calculated for temperature and salinity for points 1 and 2.

	Point 1	Point 2
Surface layer		
Temperature	0.80	0.88
Salinity	0.85	0.65
Bottom layer		
Temperature	0.91	0.49
Salinity	0.43	0.22

Both models (A4 and HRM) are quite different, so a comparison between them yields different results for the bottom layers. Nonetheless, HRM still reproduces seasonal variability (which is stronger in this case) and except for the summer, the time series are very close. In summer there is a visible influence of the fresh water sources on the shelf area, but in the other seasons the variability from both models is very similar. A simple linear correlation yields the coefficients shown in Table 2.

The best correlation coefficients are for the surface layer. This is the result of the similar atmospheric fluxes implemented in both models (S800, A4 and HRM used the same source of atmospheric forces, so we had expected to get a good correlation) and also because the forcing at the open boundaries is similar (HRM uses boundary conditions from S800 and S800 from A4). The influence of the fjord is also clear in summer. The differences, visible mostly on the temperature curves, are driven by fresh water sources.

3.3. The fjord interior

The limited availability of experimental data does not help to carry out a detailed validation of the fjord interior. Most data

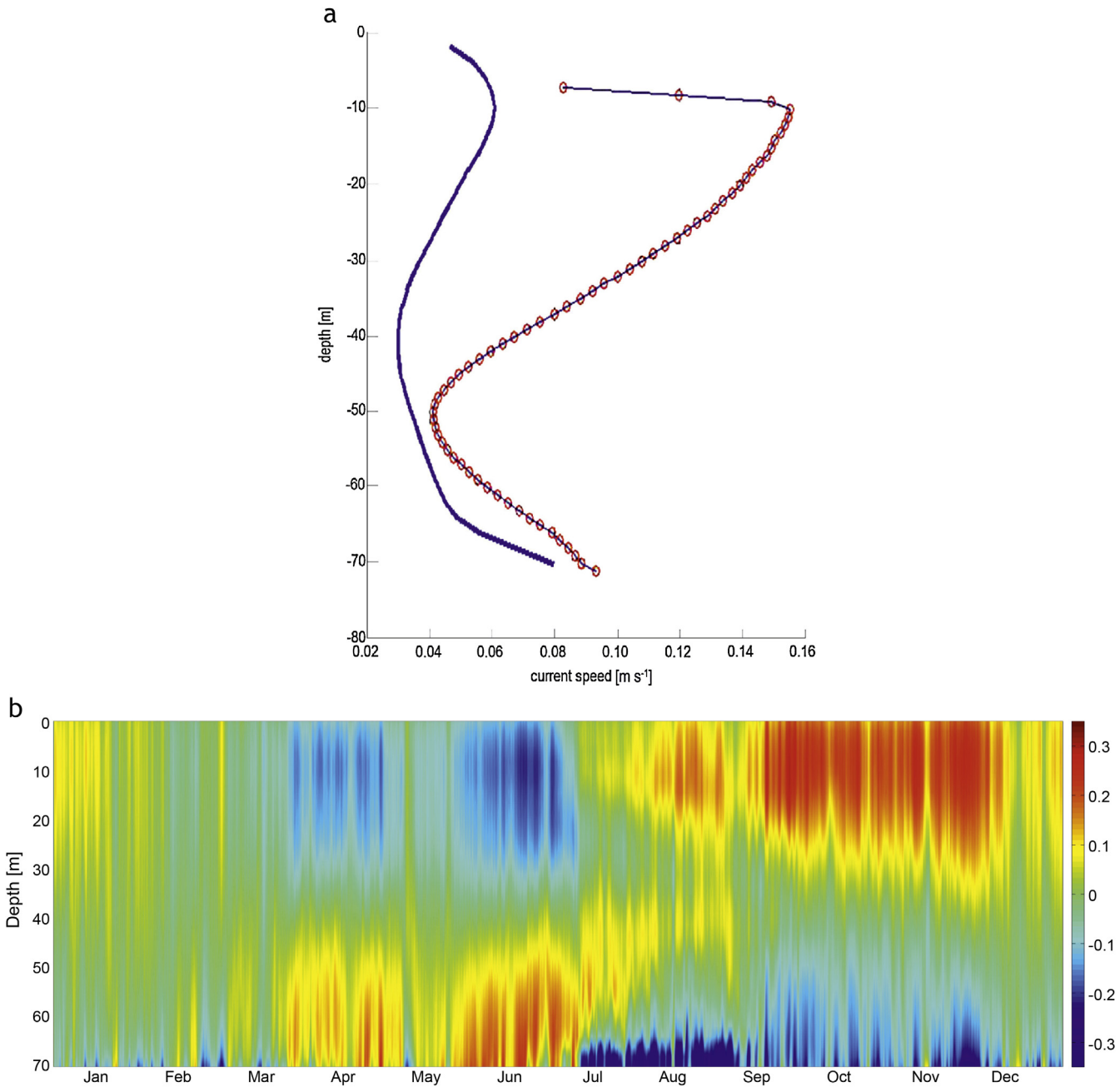

Figure 9 (a) Depth profile of the average current magnitude measured by ADCP (thin blue line with red circles) and HRM model data (thick blue line). (b) Average (for 2006—2009) temporal variability of vertical profile of current directed into Brepollen (positive value means 'into'). (For interpretation of the references to color in this figure legend, the reader is referred to the web version of this article.)

are available from the AWAKE projects (including the AWAKE-2 — Arctic Climate System Study of Ocean, Sea Ice and Glacier Interactions in the Svalbard Area) managed by the Institute of Oceanology and implemented within the framework of Polish-Norwegian collaboration. The most important time series are provided by the Norway Polar Institute's (NPI) instrument mooring located at the silled entrance to Brepollen (76.9850N 16.1728E, see Fig. 2). They were collected between September 2013 and June 2014. The mooring, equipped with a profiling current metre and a string of thermistors, was deployed at a depth of 76 m on the sill at the entrance to Brepollen and was in operation from 5 September 2013 to 5 July 2014. An AADI RDCP600 Acoustic Doppler Current Profiler was used to measure 3D currents. This instrument was mounted in a bottom frame and covered the range from ~72 m upwards with 1 m vertical resolution. It is important to add that the signal-to-noise ratio of individual current measurements decays with distance from the instrument and the upper part of the data shown in the following has large uncertainty and is included only for

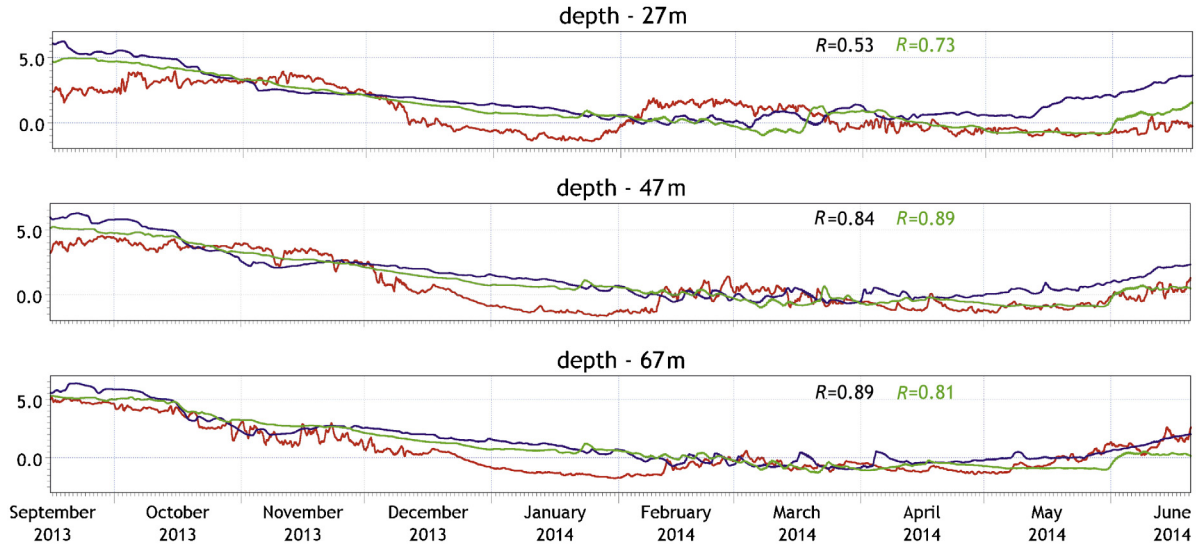

Figure 10 Temporal variability of temperature from *in situ* measurements and model simulations: red — from the thermistor string, blue and green — the HRM model (2006—2007 and 2007—2008 respectively). The location of the mooring is marked in Fig. 2 by 'M'. Linear correlation coefficients are inserted on each figure. The correlation coefficients between temperatures from the thermistors and HRM for 2006—2007 are marked in blue, and the correlation coefficients between temperatures from the thermistors and HRM for 2007—2008 in green. (For interpretation of the references to color in this figure legend, the reader is referred to the web version of this article.)

illustrational purposes. The RDCP600 was also equipped with a pressure sensor and a temperature sensor. TinyTag Aquatic2 thermistors were installed at 5 m intervals from 27 to 67 m depth. On the same rope, a HOBO U20-001-03 temperature and pressure sensor was attached at 22 m depth. The pressure sensor showed modest variation during the deployment, indicating that the thermistor chain was not seriously subducted by strong currents. Because we had no model integrations for that year, we will make a comparison for different years.

Fig. 9a shows a comparison between the average modelled current magnitude (HRM model, thick blue line) and that measured by the ADCP (left) for different depths recorded during this experiment. The result shows good compatibility between the measured and modelled velocity profile. It shows the minimum current velocity located at around 40—50 m depth. This minimum exists because of the internal tide oscillations.

In order to obtain a broader image of inflows and outflows at this location we calculated the three-year average temporal variability of currents into Brepollen (Fig. 9b — a positive velocity means 'into Brepollen'). Two main regimes are visible. The first one is between March and July. During this time the inflow into Brepollen is in the lower layer and the outflow in the upper layer. In the second one (between August and December) the inflow into Brepollen takes place in the upper layers (mostly below 30 m). The first regime ensues from the typical circulation when lighter fresh water is flowing out in the upper layers. The second one comes into existence when the volume of fresh water is negligible. This situation is typical of narrow fjords, *i.e.* when the internal Rossby deformation radius is bigger than the width of the fjord. In a such situation, water flows into the fjord in the upper layers and out in the lower layers or *vice versa*. At middle depths, the internal tidal motion is bidirectional and its average constitutes the local minimum of the magnitude.

Fig. 10 illustrates the 9 months' variability of temperature for three depths: 27, 47 and 67 m. Although the differences between the modelled and measured temperatures sometimes exceed 2 degrees, the model appears to reproduce seasonal variability quite well. Correlation coefficients are mostly over 0.8; they are smaller only for the shallowest depths. The lower correlation coefficients for 27 m depth can be explained by the low-resolution atmospheric data focused on large-scale variability (ERAi). In addition, large scale reanalysis such as ERAi does not focus on local scale processes.

4. Results and discussion

4.1. General circulation

As mentioned before, rotational effects influence the general circulation in Hornsund: this is presented in Fig. 11 as two typical circulation regimes. The figures represent the average circulation for the whole domain (temporal and depth mean) for January and July 2008, which is equivalent to the winter and summer states. For greater clarity we have used streamlines instead of vectors.

The main circulation pattern (shown in Fig. 11) represents the residual current that enters the fjord on the southern side and then recirculates along its northern part. In summer, waters of shelf origin penetrate much farther into the fjord's main basin and reach the entrance of the inner basin called Brepollen. In winter, fresh water sources are limited to

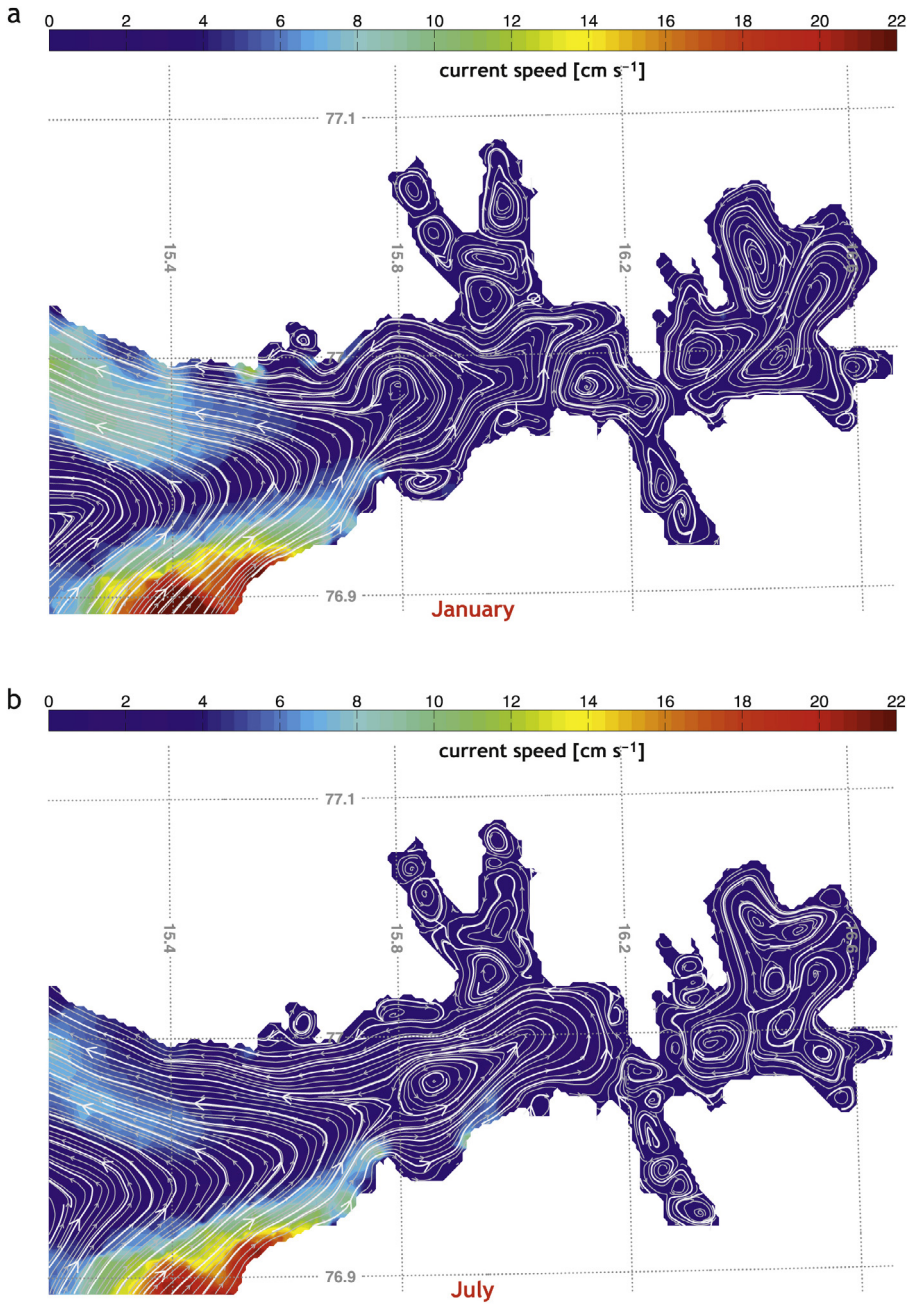

Figure 11 Streamlines (white lines) and current speed (colour-coded) over domain and time averaged in Hornsund for January (a) and July 2008 (b).

meltwater from marine terminating glaciers, thus the residual circulation pattern is similar but the volume exchange between the fjord and the shelf is much smaller than in summer (MIKE DHI does not have any assimilation data module or parameterization of ocean-glacier interaction such as surface melting or submerged plume discharge, so the representation of underwater glaciers is not possible). A cyclonic circulation is observed in the central area of the fjord mostly during the periods when fresh water inputs are the smallest. In summer this cyclonic flow is disrupted by an intense circulation driven by fresh water from terrestrial and glacial sources. The circulation in Brepollen, the easternmost part of the fjord, is also characterized by seasonal variability, with the main winter circulation pattern significantly different from that in July. Small-scale eddies in Brepollen, Samarinvagen and Burgerbukta are also more abundant in July. Increased fresh water discharge in summer results in stronger stratification in the fjord; as a consequence, submesoscale eddies are generated owing to the internal Rossby deformation radius.

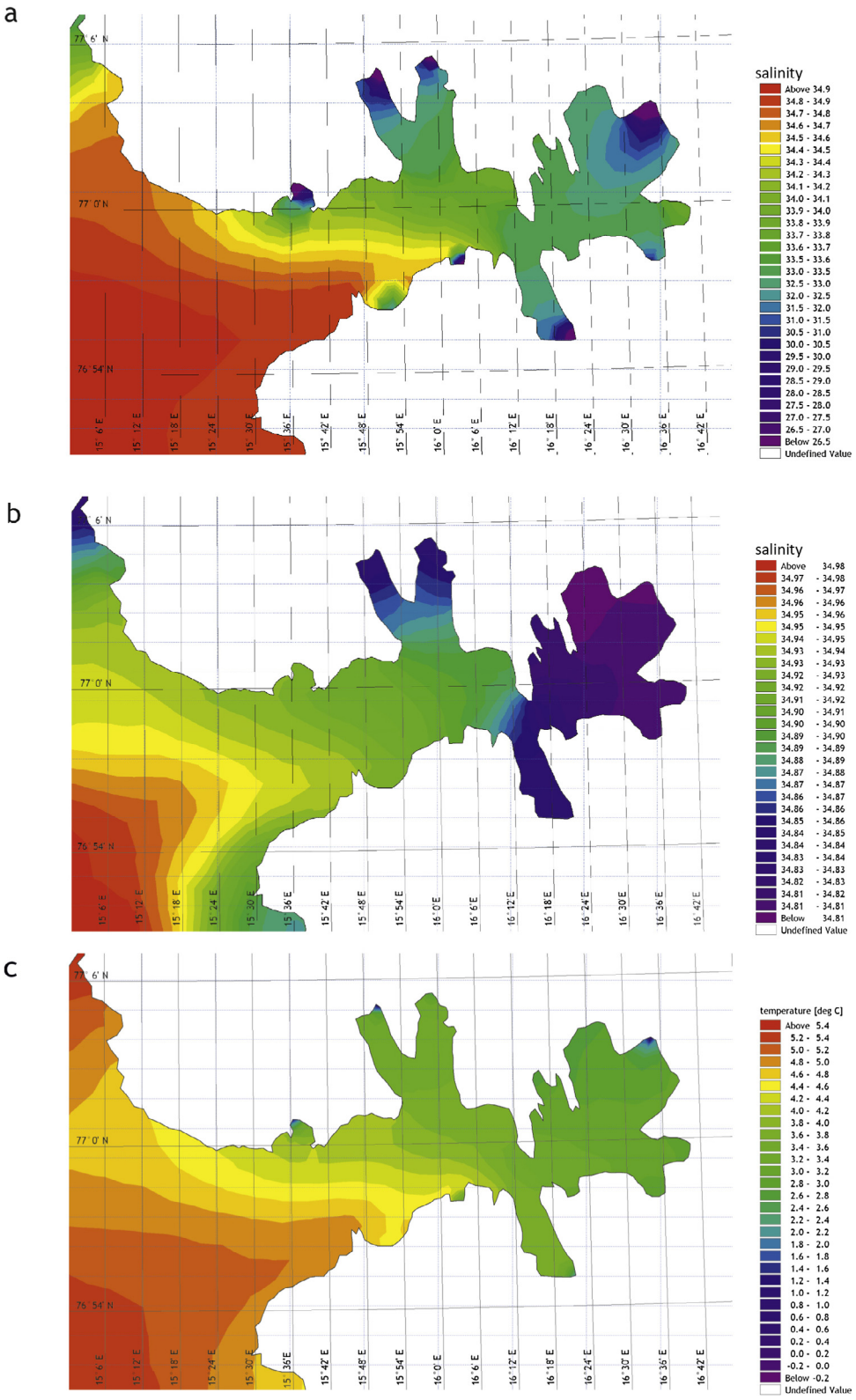

Figure 12 Average sea surface salinity (a and b) and temperature (c and d) retrieved for January (c and d) and July (a and b) 2009.

d

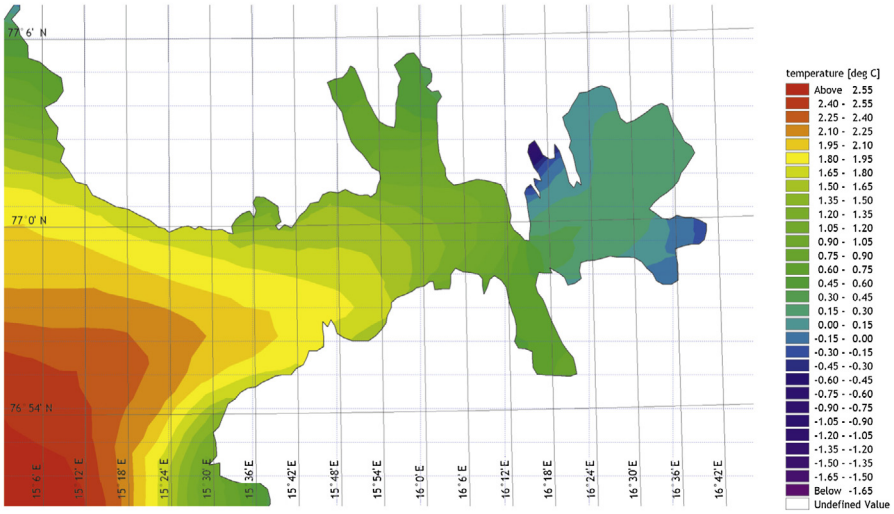

Figure 12. (*Continued*).

4.2. Hydrological front

The fjord's dynamics and fresh water from the catchment area (including the underwater glaciers, which are not included in the model) generate a hydrological front mostly at the mixed layer depth. Fronts, natural boundaries between waters of different properties, affect mixing processes, which occur in the water in both the horizontal and vertical. Dramatic changes in the properties of waters can result in the formation of various eddies, which affect local wind conditions, coastal upwelling, intrusions of intermediate waters and sea ice. The fronts may be visible on the surface as demarcation lines, colour changes, foam accumulation or choppy waters. The best indicators of the spread of riverine waters in the sea are density and salinity (Fedorov, 1986; Ginzburg and Kostianoy, 2009), but here we use temperature and salinity.

The front is represented by strong temperature and salinity gradients (Fig. 12). Fresh water from the catchment area leaves the northern area of the main fjord and oceanic water enters the fjord through the southern part of the mouth. The shape and gradient of the front depends mostly on the fresh water content in the surface layers of the fjord.

In winter this front also exists but the salinity and temperature gradients are much weaker and they are clearly symmetrical. The temperature and salinity distributions in the fjord are more homogeneous at that time and the fjord waters are generally separated from the AW of the WSC by the front, yet its shape, location and physical properties strongly depend on the season. The shape of the surface temperature and salinity fields result from the dynamic impact of the Earth's rotation on the fjord. The typical baroclinic Rossby deformation radius is 3.5–6 km for the Svalbard fjords (Cottier et al., 2010). The outer part of Hornsund is 30 km wide, which is 5–10 times greater than the internal deformation radius. The effect of rotation is better visible in the summer months, since in the warm season the strongly, vertically stratified waters tend to reduce the internal Rossby deformation radius, so the Coriolis force is more pronounced and can act more effectively in the narrower parts of the fjord as well. Fig. 13b–f shows the sections marked in Fig. 13a. The first one (IP1-IP2-IP3-IP4-IP5) is along the fjord (we call it the along-fjord section (HS)), while the second one is across the fjord entrance (A-A′, the cross-section (VS)). At the HS an area is visible in the middle depths with a strong salinity and temperature gradient (at about 20 m depth) – above this depth the fresh water from the catchment area flows out in the surface layers of the fjord. The waters are mixed, and the degree of mixing depends on the distance from the source and local dynamic conditions. The VSs show that the main core of the shelf waters enters the southern mouth area. Moreover, the image showing the velocities of VS (which represents the velocity of inflow – a positive value means that the flow is directed into the fjord) confirms that the main outflow area is in the upper and lower layers and is closer to the northern part of the fjord. As mentioned earlier, the shape of the front depends on the fresh water content in the fjord and could be very useful for estimating the amount of fresh water from glaciers and the catchment area. We will be able to formulate more general conclusions about the hydrological front and the impact of other factors on front formation following a detailed analysis of the front over a longer period of time; this is planned for the near future.

4.3. Salt and heat content and its anomaly of the main fjord and Brepollen

The fjord's dynamics strongly depend on the season. The annual variability could be represented by the fjord's heat and salt content. Furthermore, the fjord is known to be under the strong influence of shelf waters consisting of WSC and SC, and it is impossible to separate them because these two currents mix at the fjord's mouth (Gluchowska et al., 2016; Walczowski, 2013). Analysis of the salt and

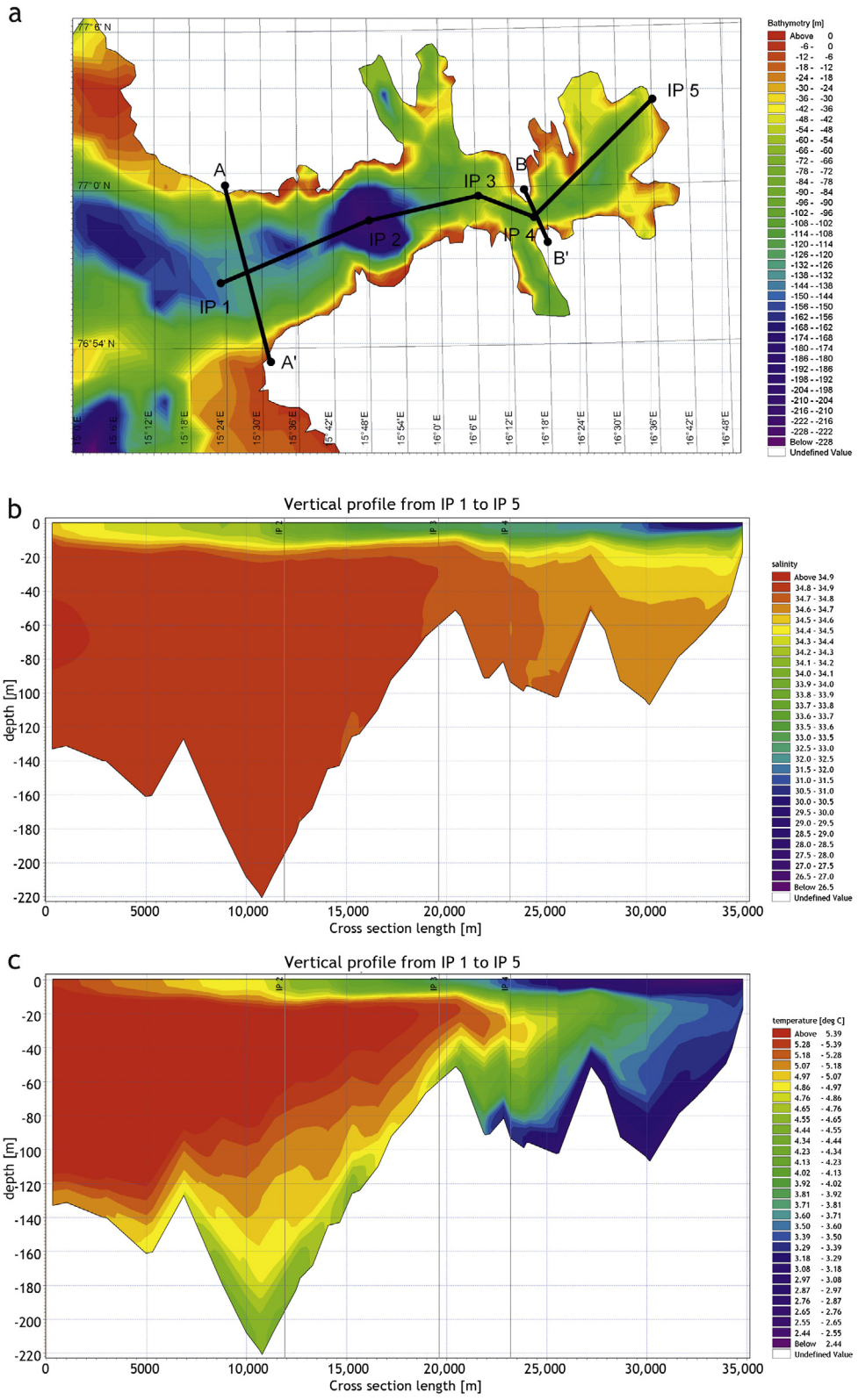

Figure 13 Vertical sections of salinity, temperature and velocity towards the fjord for July; (a) locations of the sections; section IP1-IP2-IP3-IP4-IP5 of salinity (b) and temperature (c); sections A-A′ of salinity (d), temperature (e) and velocity directed towards the fjord (f). Section IP1-IP2-IP3-IP4-IP5 is called along-fjord (HS), sections A-A′ and B-B′ are called cross-sections (VS). Cross-sections are shown with north on the left-hand side (i.e.points A or B from panel a)). Positive velocity on the subplot (f) is directed into the fjord. Sections A-A′ and B-B′ are also presented for discussion in the subsection 'Salt and heat content and its anomaly in the main fjord and Brepollen' and in Fig. 16.

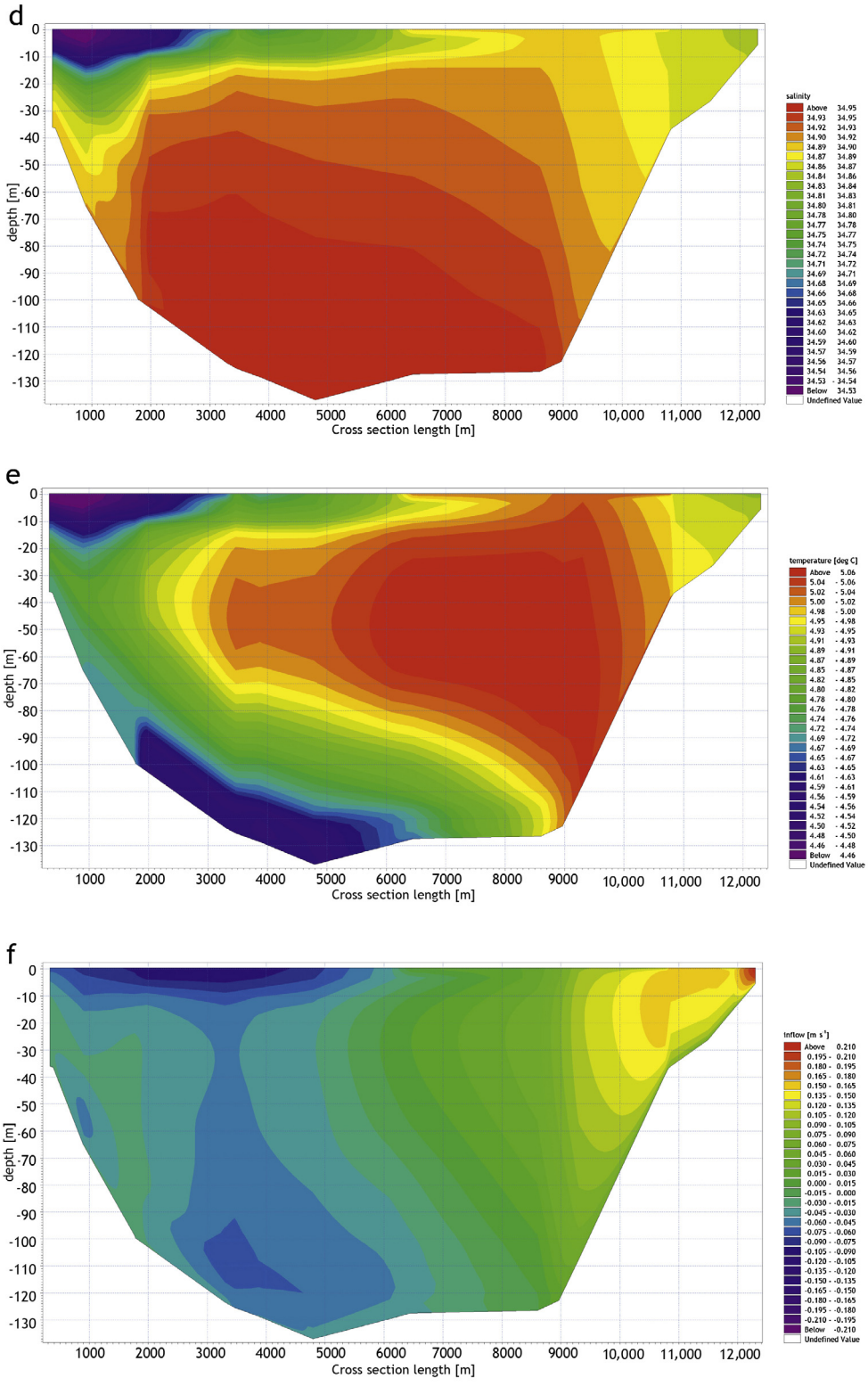

Figure 13. (*Continued*).

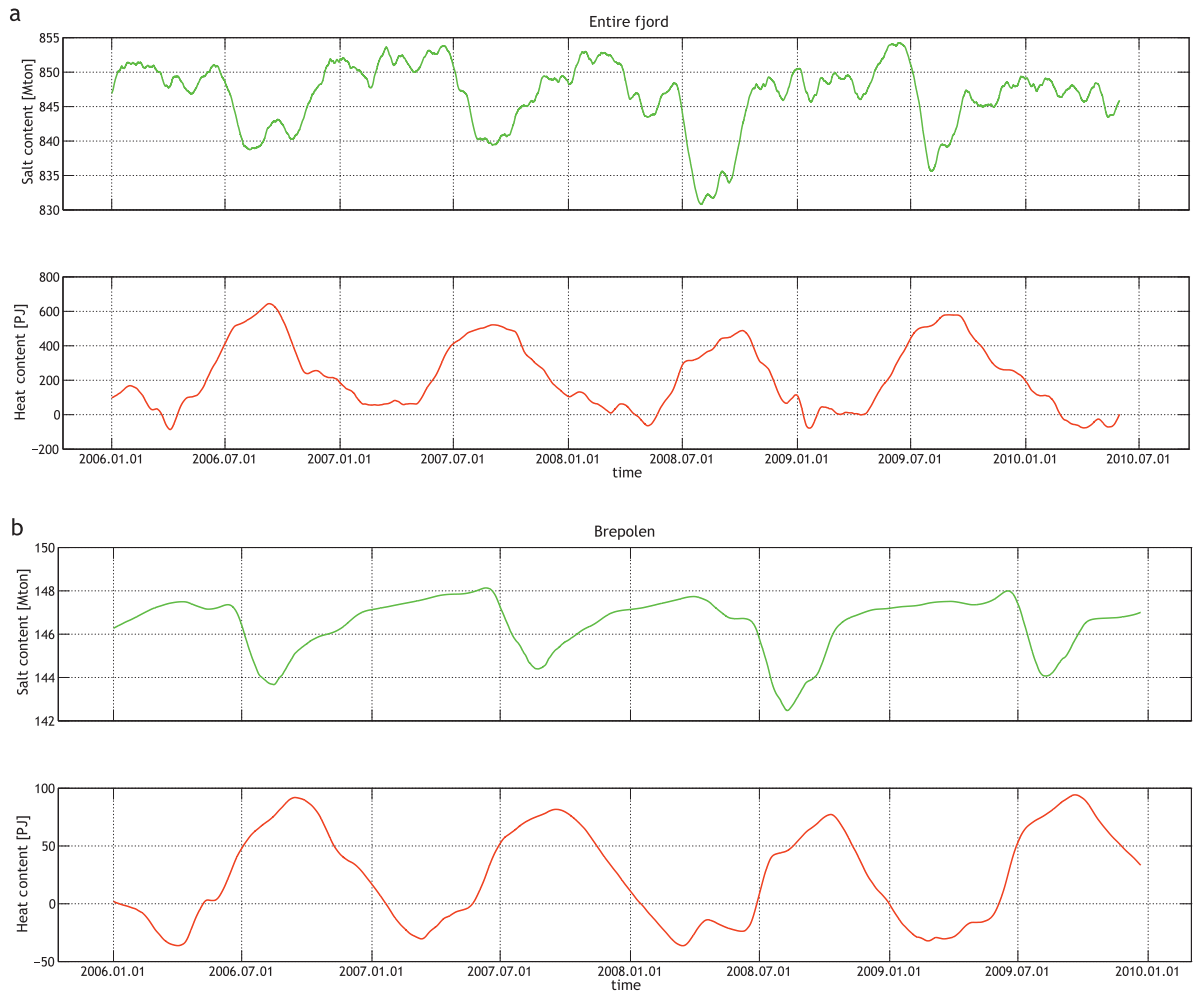

Figure 14 Heat and salt content for the entire fjord (a) and Brepollen (b) for the period 01.01.2006—31.12.2009.

heat content in the whole fjord shows the clearly visible seasonal variability in the heat and salt content of the entire fjord and Brepollen (Fig. 14) (note: the reference temperature for the heat content was taken to be 0.1°C). Moreover, any increase in the salt content during any part of the year, except during periods of decreasing catchment area activity, which begins in mid-July (see Fig. 4c), means that it is mostly under the influence of WSC. Fig. 15 shows the salt content anomaly (SCA) integrated over time. The anomaly was integrated because this process removes all small oscillations. For example, if the anomaly is represented by a simple sine function, through oscillation, the time integrated sine will yield zero in the long-term. On the other hand, it works like a low pass filter. The salt anomaly integrated over time (and its derivative — Eqs. (2) and (3) for the entire fjord provides no evidence that only WSC or only SC (Fig. 15) exert an influence there. However, Fig. 16 shows that the method detects inflows of more saline or fresher water into the fjord or Brepollen, but it is still difficult to say whether Hornsund is under the influence of only one of them.

$$\Theta_A(t) = \int_0^t (\Theta(t') - \overline{\Theta}) dt', \tag{2}$$

$$\Theta'_A(t) = \frac{d\Theta_A}{dt}, \tag{3}$$

where Θ is the tracer, t the time, and $\overline{\theta}$ the time averaged tracer.

Separating the inflows of WSC and SC in Hornsund appears to be impossible. But for Brepollen the anomalies are very stable and there is a strong seasonal variability. The inference is that the circulation is stable but that it can be disturbed by fresh water from the catchment area and glaciers. Consequently, at this time scale, the circulation supplies additional heat and transfers salt from the shelf area into Brepollen and the entire fjord. Furthermore, it transfers additional salt and heat to the main fjord area, but this is small compared to the short time scale of natural variability associated with inflows from the shelf. As shown in Fig. 15, the variability in the

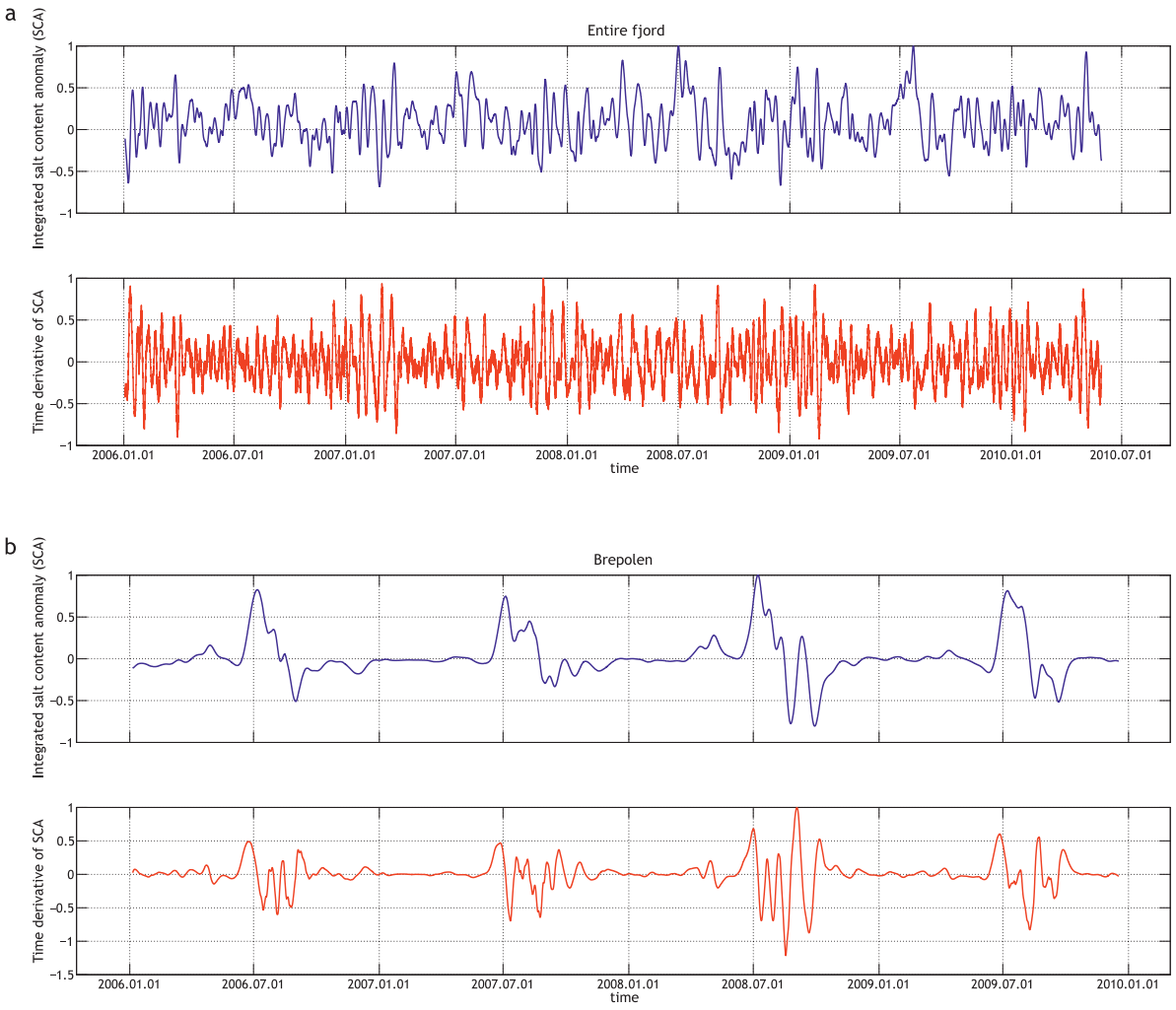

Figure 15 The SCA (over time) and its derivative for the entire fjord (a) and the Brepollen area (b) for the period 01.01.2006–31.12.2009.

salt content is related to inflows of more saline or fresher water into Brepollen. The atmospheric influence on the salt content can be neglected. Precipitation represents a very small amount of the fresh water from the catchment area, and other atmospheric factors are unrelated to the integrated salt content. Other factors that could have some influence on the salt content are underwater glaciers. But as we stated above, we are unable to construct even a simple representation of the glacier, so we should not analyze the influence of heat content. SCA in the Brepollen shows a strong seasonal variability which depends strongly on fresh water discharge. Although the fresh water discharge for every year is identical, the SCAs are different (Fig. 15). As mentioned above, we do not think that atmospheric factors could have a strong influence on this. Only shelf waters consisting of mixed WSC and SC could change the shape of SCA. Fig. 16 shows sections B-B′ (shown in Fig. 13a) on the positive and negative representation of SCA (also for the positive and negative time derivative of SCA). It is clear that increasing (as well as decreasing) SCA is caused by inflows of more saline waters from the main fjord to Brepollen. The time derivative of SCA is more sensitive than SCA and it is much easier to detect inflows of more saline (or fresher) water into Brepollen.

5. Concluding remarks

A hydrodynamic model has been implemented for the west Svalbard fjord Hornsund. HRM reproduces seasonal variability of the fjord properly. Validation of the model shows quite good agreement between the available data and the model results. The general circulation is shown, based on the model integrations. Generally, the fjord circulation can be divided into two regimes, one representing the winter circulation, the other being related to summer and strongly linked to fresh water discharges. Furthermore, the fjord's hydrodynamic front has been documented. Seasonal variability is also presented for the heat and salt content. Analysis of the integrated salt content anomaly suggests that apart from the strong seasonal periodicity driven by shelf waters, rela-

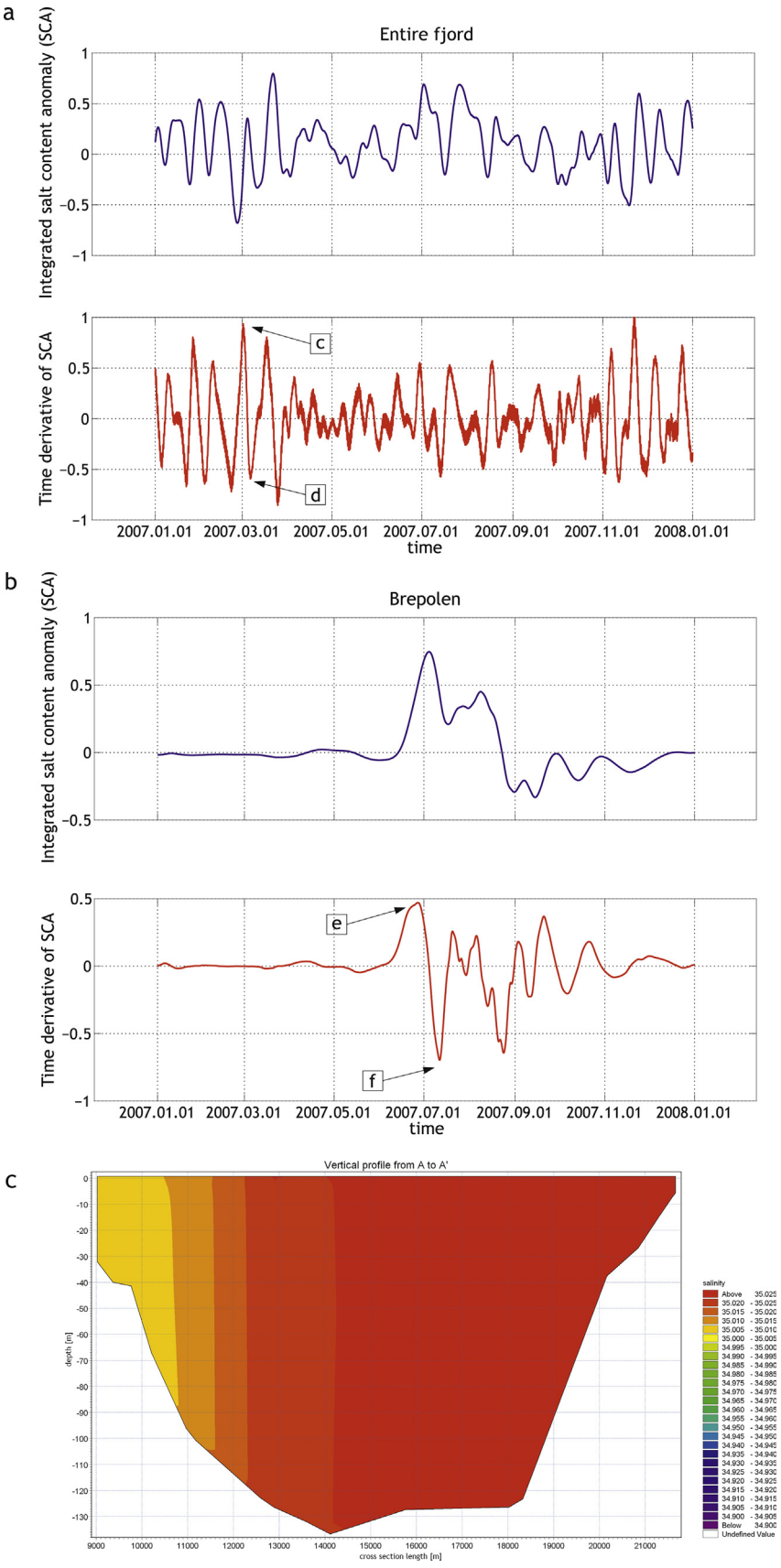

Figure 16 Zoomed, time-integrated salt anomaly for the entire fjord and the Brepollen area, and sections (c, d, e, f) representing the inflows of saline and fresh water (the time location on the chart is also marked on subplots (a) and (b)), sections are marked in Fig. 13a (A-A′ and B-B′). The results are for 2007.

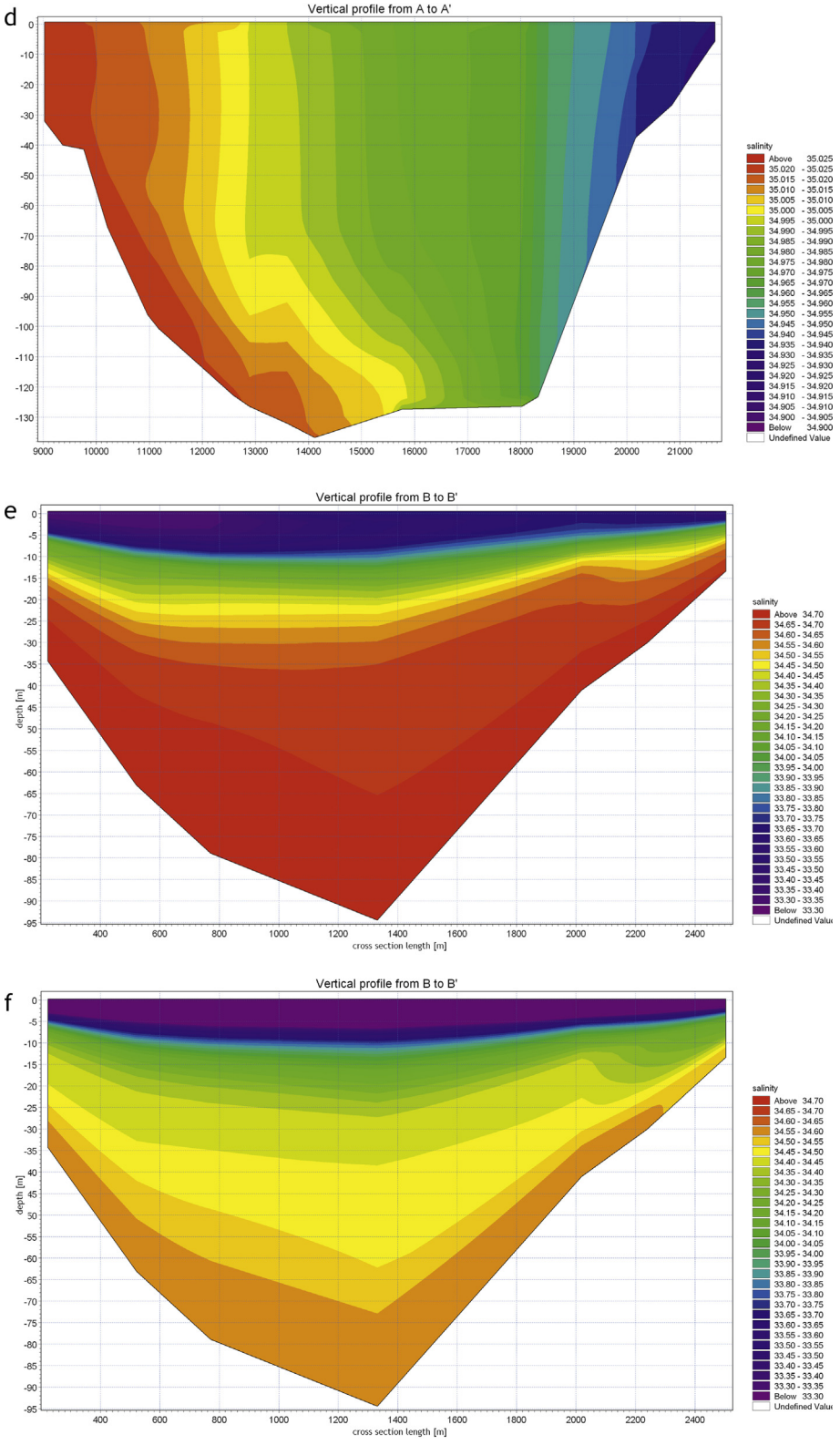

Figure 16. (*Continued*).

tively large amounts of salt and heat are transported into Brepollen when water from the catchment area is carried into the fjord.

The model has also some drawbacks. It does not incorporate any ice model, so it uses only external data. This means there is no fresh water generated during ice melting. The same problem also arises when ice forms. Freezing does not introduce any saline water into the fjord. Ice cover in the model is treated only as a barrier between atmospheric forces and the fjord surface, modifying only momentum and heat fluxes. Furthermore, in an Arctic fjord it is important to include underwater glaciers. But DHI does not provide any module that could help create such glacier walls in the model. The inclusion of these processes would probably decrease heat content in the fjord and would increase salt content. We think that it could also have some influence on the general circulation of the fjord as well as on the shape, salinity and temperature gradient in the hydrological front.

We are planning to include in our future work underwater glaciers (in the first step in basic form as an underwater wall that has no salinity or freezing temperature). After that we intend to investigate the hydrological front more deeply, include more realistic winds (data from ECMWF are close to the geostrophic wind, but the main wind in the Hornsund area approximates a sea breeze) and analyze the influence of factors affecting climate change.

Acknowledgements

We are very grateful to Prof. Andrzej Jankowski for his advice and the helpful, stimulating discussion.

The project was co-financed from the funds of the Leading National Research Centre (KNOW) received by the Centre for Polar Studies for the period 2014—2018.

This work was also partially carried out within the framework of projects GAME (DEC-2012/04/A/NZ8/00661) and AWAKE2 (Pol-Nor/198675/17/2013).

Data from the A4 and S800 models were made available through the Fram Centre 'Arctic Ocean' flagship project 'ModOIE'.

References

Albretsen, J., Hattermann, T., Sundfjord, A., 2017. Ocean and sea ice circulation model results from Svalbard area (ROMS) [Data set]. Norwegian Polar Institute, http://dx.doi.org/10.21334/npolar.2017.2f52acd2.

Błaszczyk, M., Jania, J., Kolondra, L., 2013. Fluctuations of tidewater glaciers in Hornsund Fjord (Southern Svalbard) since the beginning of the 20th century. Pol. Polar Res. 34 (4), 327—352, http://dx.doi.org/10.2478/popore-2013-0024.

Budgell, W.P., 2005. Numerical simulation of ice-ocean variability in the Barents Sea region: towards dynamical downscaling. Ocean Dynam. 55 (3), 370—387, http://dx.doi.org/10.1007/s10236-005-0008-3.

Chassignet, E.H., Hurlburt, H.E., Smedstad, O.M., Halliwell, G.R., Hogan, P.J., Wallcraft, A.P., Bleck, R., 2006. Ocean prediction with the hybrid coordinate ocean model (HYCOM). In: Chassignet, E.P., Verron, J. (Eds.), Ocean Weather Forecasting. Springer, Dordrecht, 577 pp., http://dx.doi.org/10.1007/1-4020-4028-8.

Cottier, F.R., Nilsen, F., Skogseth, R., Tverberg, V., Skarthhamar, J., Svendsen, H., 2010. Arctic fjords: a review of the oceanographic environment and dominant physical processes. Geol. Soc. London, Spec. Publ. 344 (1), 35—50, http://dx.doi.org/10.1144/SP344.4.

Cottier, F., Tverberg, V., Inall, M., Svendsen, H., Nilsen, F., Griffiths, C., 2005. Water mass modification in an arctic fjord through cross-shelf exchange: the seasonal hydrography of kongsfjorden, Svalbard. J. Geophys. Res. 110 (C12), 18 pp., http://dx.doi.org/10.1029/2004JC002757.

Counillon, F., Sakov, P., Bertino, L., 2010. Development of TOPAZ4 prototype. In: EGU General Assembly Conference Abstracts.

Dee, D.P., Uppala, S.M., Simmons, A.J., Berrisford, P., Poli, P., Kobayashi, S., Andrae, U., Balmaseda, M.A., Balsamo, G., Bauer, P., Bechtold, P., Beljaars, A.C.M., van de Berg, L., Bidlot, J., Bormann, N., Delsol, C., Dragani, R., Fuentes, M., Geer, A.J., Haimberger, L., Healy, S.B., Hersbach, H., Hólm, E.V., Isaksen, L., Kållberg, P., Köhler, M., Matricardi, M., McNally, A.P., Monge-Sanz, B.M., Morcrette, J.J., Park, B.K., Peubey, C., de Rosnay, P., Tavolato, C., Thépaut, J.N., Vitart, F., 2011. The ERA-Interim reanalysis: configuration and performance of the data assimilation system. Quarter. J. R. Meteorol. Soc. 137 (656), 553—597, http://dx.doi.org/10.1002/qj.828.

Egbert, G.D., Erofeeva, S.Y., 2002. Efficient inverse modeling of barotropic ocean tides. J. Atmos. Ocean. Technol. 19, 183—204, http://dx.doi.org/10.1175/1520-0426(2002)019<0183:EIMOBO>2.0.CO;2.

Fedorov, K.N., 1986. The Physical Nature and Structure of Oceanic Fronts. Springer-Verlag, New York, 333 pp.

Flather, R.A., 1976. A tidal model of the northwest European continental shelf. Mem. Soc. Roy. Sci. Liege 6 (10), 141—164.

Frankowski, M., Zioła-Frankowska, A., 2014. Analysis of labile form of aluminum and heavy metals in bottomsediments from Kongsfjord, Isfjord, Hornsund fjords. Environ. Earth Sci. 71 (3), 1147—1218, http://dx.doi.org/10.1007/s12665-013-2518-5.

Ginzburg, A.I., Kostianoy, A.G., 2009. Front and mixing processes. Oceanography 1, 7 pp.

Gluchowska, M., Kwasniewski, S., Prominska, A., Olszewska, A., Goszczko, I., Falk-Petersen, S., Hop, H., Weslawski, J.M., 2016. Zooplankton in Svalbard fjords on the Atlantic-Arctic boundary. Polar Biol. 39 (10), 1—18, http://dx.doi.org/10.1007/s00300-016-1991-1.

Haidvogel, D.B., Arango, H., Budgell, W.P., Cornuelle, B.D., Curchitser, E., Di Lorenzo, E., Fennel, K., Geyer, W.R., Hermann, A.J., Lanerolle, L., Levin, J., McWilliams, J.C., Miller, A.J., Moore, A. M., Powell, T.M., Shchepetkin, A.F., Sherwood, C.R., Signell, R.P., Warner, J.C., Wilkin, J., 2008. Ocean forecasting in terrain-following coordinates: formulation and skill assessment of the Regional Ocean Modeling System. J. Comp. Phys. 222 (7), 3595—3624, http://dx.doi.org/10.1016/j.jcp.2007.06.016.

Hattermann, T., Isachsen, P.E., von Appen, W.-J., Albretsen, J., Sundfjord, A., 2016. Eddy-driven recirculation of Atlantic Water in Fram Strait. Geophys. Res. Lett. 43 (7), 3406—3414, http://dx.doi.org/10.1002/2016GL068323.

Jeżowiecka-Kabsch, K., Szewczyk, H., 2001. Mechanika płynów. Oficyna Wyd. Politech. Wroc., Wrocław, 386 pp.

Kantha, L.H., Clayson, C.A., 2000. Numerical Models of Oceans and Oceanic Processes. Acad. Press, San Diego, 750 pp.

Kowalik, Z., Marchenko, A., Brazhnikov, D., Marchenko, N., 2015. Tidal currents in the western Svalbard Fjords. Oceanologia 57 (4), 318—332, http://dx.doi.org/10.1016/j.oceano.2015.06.003.

Lien, V.S., Vikebø, F.B., Skagseth, Ø., 2013. One mechanism contributing to co-variability of the Atlantic inflow branches to the Arctic. Nat. Commun., http://dx.doi.org/10.1038/ncomms2505 Art No. 1488.

MIKE_DHI, 2014. MIKE 21 Toolbox. Global Tide Model — Tidal Prediction. DHI, Hørsholm, 20 pp.

MIKE and Doc. 2010—2014. MIKE 21 & MIKE 3 Flow Model FM. Hydrodynamic Module, Sci. Doc., DHI, Hørsholm, 14 pp.

Nilsen, F., Cottier, F., Skogseth, R., Mattsson, S., 2008. Fjord—shelf exchange controlled by ice and brine production: the interannual

variation of Atlantic Water in Isfjorden, Svalbard. Cont. Shelf Res. 28 (14), 1838—1853, http://dx.doi.org/10.1016/j.csr.2008.04.015.

Sakov, P., Counillon, F., Bertino, L., Lisæter, K.A., Oke, P.R., Korablev, A., 2012. TOPAZ4: an ocean-sea ice data assimilation system for the North Atlantic and Arctic. Ocean Sci. 8 (4), 633—656, http://dx.doi.org/10.5194/os-8-633-2012.

Shchepetkin, A.F., McWilliams, J.C., 2009. Correction and commentary for "Ocean forecasting in terrain-following coordinates: formulation and skill assessment of the regional ocean modeling system" by Haidvogel et al. J. Comp. Phys. 228 (24), 8985—9000, http://dx.doi.org/10.1016/j.jcp.2009.09.002.

Węsławski, J.M., Koszteyn, J., Zajaczkowski, M., 1995. Fresh water in Svalbard fjord ecosystems. In: Skjodal, H.R., Hopking, C., Erikstad, K.E., Leinaa, H.P. (Eds.), Ecology of Fjords and Coastal Waters. Elsevier, Amsterdam, 229—241.

Walczowski, W., 2007. Warm anomalies propagation in the west spistbergen current. Probl. Klimatol. Polar. 17, 71—76, (in Polish with English summary).

Walczowski, W., 2013. Frontal structures in the West Spitsbergen Current margins. Ocean Sci. 9 (6), 957—975, http://dx.doi.org/10.5194/os-9-957-2013.